Effective energy window of the *E*1 photon strength function for astrophysical neutron-capture reaction rates

Bing Wang [1], Yi Xu,[2,*] and Xiaodong Tang [1,†]

[1]*Institute of Modern Physics, Chinese Academy of Sciences, Lanzhou 730000, China*

[2]*Extreme Light Infrastructure - Nuclear Physics (ELI-NP), Horia Hulubei National Institute for R&D in Physics and Nuclear Engineering (IFIN-HH), 077125 Bucharest-Magurele, Romania*

The electric-dipole (*E*1) photon strength function (PSF), which is a key input in the statistical model calculations for astrophysical neutron-capture reaction rates, has been studied with a focus on the important energy ranges of the emitting γ rays. Comparing the available experimental data of the *E*1 PSF with the strength predicted by microscopic models, we find that the uncertainties in the *E*1 PSF below the neutron separation energy have a great impact on the neutron-capture reaction rates. A further study on the sensitivities of the reaction rate to the variations of the *E*1 PSF at different γ-ray energies indicates that there is an effective energy window in which the *E*1 PSF contributes greatly to the neutron-capture reaction rates. We propose two functions to describe this window, which can be applied to the nuclei with dominant transitions to the continuum levels and is applicable to the general astrophysical environments of neutron captures. Employing the Gaussian approximation function of the effective window, we can conveniently get several specific effective energy ranges according to the contributions to the astrophysical rate. It is found that currently available experimental data of the *E*1 PSF do not completely cover these important energy ranges. Further theoretical and experimental studies are needed in the proposed energy ranges to improve the descriptions of the *E*1 PSFs.

I. INTRODUCTION

About half of the nuclei with $A > 60$ observed in nature are formed by the rapid neutron-capture process (*r*-process) occurring in explosive stellar events [1]. The *r*-process is believed to take place in environments characterized by high neutron density ($N_n > 10^{20}$ cm^{-3}), so that successive neutron captures proceed into neutron-rich regions well off the β stability valley forming exotic nuclei that cannot be produced and therefore studied in the laboratory. When the temperature or the neutron density required for the *r*-process is low enough to break the equilibrium of (n, γ)-(γ, n), the distribution of the *r*-process abundance depends directly on the neutron capture rates of the so-produced exotic neutron-rich nuclei [2]. Carbon-enhanced metal-poor (CEMP) r/s stars demonstrate surface-abundance distributions characteristic of the nucleosynthesis of the intermediate neutron capture process (*i*-process). About 70% of the neutron-capture rates involved during *i*-process nucleosynthesis are not known experimentally. It is found that the uncertainties of these unknown capture reaction rates introduce significant discrepancies in the predicted surface abundance enrichment of the AGB star, especially for the isotopes in the $75 < Z < 80$ region [3,4]. The neutron-capture rates are commonly evaluated within the framework of the statistical model of Hauser-Feshbach, which

makes the fundamental assumption that the capture process takes place with the intermediary formation of a compound nucleus in thermodynamic equilibrium [5]. In this approach, the Maxwellian-averaged neutron-capture rate at temperatures of relevance in *r*-process or *i*-process environments strongly depends on the PSF.

Over the past decades, a large number of experimental efforts have been devoted to measure photon strength functions (PSFs) by using the photon, neutron, and charged-particle beams [6,7]. Quite often, different experimental techniques have led to discrepant results, so a coordinated effort has been made to compile and assess the existing experimental data on PSFs from the giant dipole resonance region to energies below the neutron separation energy [8]. However, there are still considerable uncertainties in the experimental data for PSFs, especially at the energies around or below the neutron separation energy which are critically important for astrophysical neutron-capture reaction rates.

Large-scale calculations of the dipole PSF have traditionally been performed on the basis of the phenomenological Lorentzian model [8,9]. The Lorentzian model and its generalized forms are widely used to describe experimental data well with conveniently adjustable parameters. However, this approach is unable to predict the enhancement of the dipole PSF at low energies and lacks reliability when dealing with exotic nuclei [8]. On the other hand, the reliability of large-scale predictions of the dipole PSF can be greatly improved by the use of microscopic (or semimicroscopic) models [10–14]. Combined with the simple analytical expressions to account

---

for the missing strength at the lowest energies approaching zero, the microscopic approach based on the finite-range D1M Gogny force is quite successful in describing the low-energy enhancement [15] and effectively explaining the experimental results from the Oslo-type experiments [16–18]. Provided satisfactory reproduction of available experimental data, the more microscopic the underlying theory, the greater the confidence in the extrapolations out towards the experimentally unreachable regions. Nevertheless, microscopic approaches also have some limitations, such as the fine tuning required to accurately reproduce a large experimental data set, which is very delicate and time consuming.

The $E1$ transition generally dominates the electromagnetic transition of the nuclei, and the uncertainties of the $E1$ PSF in experimental measurements and theoretical predictions prevent us from giving a sufficiently accurate description of the astrophysical neutron-capture reaction rates. According to the description of Hauser-Feshbach model, it is known that the astrophysical neutron-capture reaction rate is mainly governed by the γ width which strongly depends on the PSF, as the larger particle width cancels with the total width, leaving only the smaller γ width remaining [19]. Therefore, it is quite necessary to quantify the impacts of the uncertainties in PSFs on the astrophysical rates. Furthermore, it is expected to obtain an effective energy window of the $E1$ PSF, which can suggest to both nuclear experimentalists and theoreticians to focus on improving the uncertainties of the PSF in the most important γ-ray energy.

In this paper, we investigate the impact of the uncertainties in the $E1$ PSF on the astrophysical neutron-capture reaction rates, and analyze the sensitivities of the reaction rates to the variations of the $E1$ PSF at different γ-ray energies. An effective energy window is proposed to describe the effective energy range in which the $E1$ PSF has great contributions to the neutron-capture reaction rate. All relevant calculations of the cross section and the reaction rate about the neutron-capture reaction are performed within the framework of the Hauser-Feshbach statistical model using the TALYS reaction code [20–22]. The rest of this article is organized as follows. In Sec. II, the uncertainties of the $E1$ PSF and the sensitivities of the reaction rate to the variations of the $E1$ PSF are analyzed. In Sec. III, the effective energy window is proposed and discussed. In Sec. IV, the conclusions are given.

II. UNCERTAINTIES AND SENSITIVITIES ABOUT THE $E1$ PSF

A. Impact of the uncertainties in the $E1$ PSF on the reaction rate

In order to investigate how much the uncertainties in the $E1$ PSF impact on the reaction rate, we will analyze this problem using available experimental data below the neutron separation energy acquired from the PSF database provided by the International Atomic Energy Agency (IAEA) [23], and their corresponding microscopic theoretical predictions.

In the astrophysical environment, due to the very low incident energy compared with the Q value in a neutron-capture reaction, the maximum value of the γ-decay energy is generally around the neutron separation energy. Various

experimental methods can be used to measure $E1$ PSFs below the neutron separation energy, such as the discrete resonance capture (DRC) method, the inelastic proton scattering (PP) method, and the nuclear resonance fluorescence (NRF) method [8]. The experimental data obtained from these approaches, along with the theoretical predictions of the microscopic Hartree-Fock-Bogoliubov (HFB) plus quasi-particle random-phase approximation model, based on the BSk7 Skyrme force (BSk7 + QRPA) [11] and the D1M Gogny force (D1M + QRPA) complemented by low-energy enhancement [15], are both shown in Fig. 1. In the energy ranges where the experimental data are available, differences between the predictions and the experimental results can still be found. Below the neutron separation energy, both microscopic predictions exhibit a similar increasing trend with rising energies, except for the lowest energies just above zero where an enhancement is added to the D1M PSF. To assess the impact of the uncertainties in the $E1$ PSF on the astrophysical rate, we combine the BSk7 + QRPA predictions and the experimental data by two schemes, as shown in Fig. 1. Considering that the theoretical extrapolation out towards unknown regions often relies on the data points at the tails of the experimental data, we adopt a scheme (Scheme I) that employs experimental data when available, and, out of the experimental energy range, scales the microscopic prediction respectively to the last point at each end of experimental data. On the other hand, to see the consequences derived from the discrepancy between the theoretical and experimental results, we adopt another scheme (Scheme II) that employs the experimental data when available, and when no data exist, the microscopic predictions are directly employed.

Figure 2 shows the ratios of neutron-capture reaction rates calculated with the two schemes of the $E1$ PSF described in Fig. 1, respectively, to the one calculated with the BSk7 + QRPA predictions. It can be seen that reaction rates calculated by Scheme I with a combination of the experimental data and the extrapolations are generally larger than the results of using the microscopic PSF by a factor ranging from one to four, and for the nucleus ^{54}Cr even up to 20 times. The differences of the reaction rates between using Scheme II by inserting the experimental data into the microscopic prediction and using only the microscopic PSF are also remarkable, and apparently these differences are partially depend on the number of experimental data points.

NRF method aims at determining the photoabsorption cross section and the total dipole PSF through the photon scattering experiments. It provides some experimental data of the total dipole PSF below the neutron separation energy. From these data, We can extract the $E1$ PSF f_{E1} using an empirical expression proposed by the RIPL-3 library [9],

$$f_{E1}/f_{M1} = 0.0588 \cdot A^{0.878}, \qquad (1)$$

where f_{M1} is the magnetic-dipole ($M1$) PSF, and A is the atomic mass. The resulting $E1$ PSFs extracted from the NRF data are shown in Fig. 3. As in Fig. 2, the theoretical predictions from the microscopic model and the results from Schemes I and II are also shown in Fig. 3. As can be seen, there are also differences between the experimental data extracted from the NRF approach and the theoretical predictions.
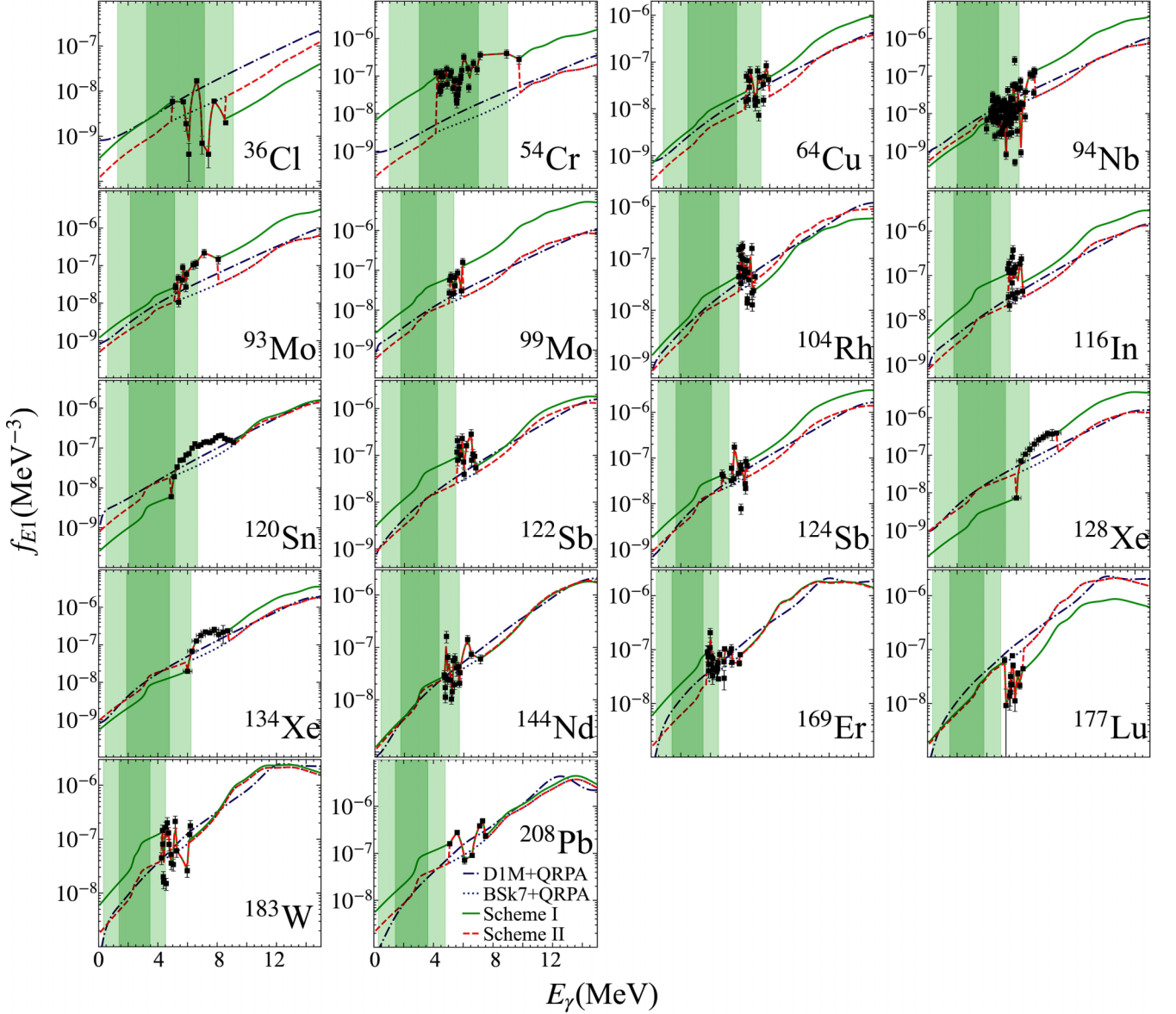
FIG. 1. Comparisons between the theoretical $E1$ PSFs and the experimental data. Between the experimental data points (black squares) the linear interpolations are implemented for continuity. Dotted and dash-dotted lines are the microscopic theoretical $E1$ PSFs based on the Skyrme force and the Gogny force, respectively. Green solid lines (Scheme I) and red dashed lines (Scheme II) are two schemes that combine the theoretical and the experimental results. Dark and light green shaded areas are the effective energy ranges at $[E_0 - \sigma, E_0 + \sigma]$ and $[E_0 - 2\sigma, E_0 + 2\sigma]$, respectively. Experimental data are taken from Refs. [25–39].

Correspondingly, the ratios of neutron-capture reaction rates calculated with the $E1$ PSFs of Schemes I and II, respectively, to the one calculated with the BSk7 + QRPA PSF are shown in Fig. 4. It is found that the uncertainties in the $E1$ PSF derived from NRF data also have a great impact on the reaction rates with ratios ranging from one to four.

B. Sensitivities of the reaction rate to the $E1$ PSF

Significant impacts of the uncertainties in the $E1$ PSF on neutron-capture reaction rates are found as described in Sec. II A. However, it is not clear which energy range of the

$E1$ PSF can give the major contributions to the astrophysical neutron-capture reaction rate.

In order to quantify the impact of a variation of a model quantity q on the final calculated results Ω, the relative sensitivity Ω_{S_q} is defined in Ref. [24] as

$$\Omega_{S_q} = \frac{v_\Omega - 1}{v_q - 1}, \qquad (2)$$

where $v_\Omega = \Omega_{\text{new}}/\Omega_{\text{old}}$ is a changed factor in Ω as a result of a change in q by the factor of $v_q = q_{\text{new}}/q_{\text{old}}$. Relative sensitivities of the astrophysical neutron-capture reaction rates to the variations of the $E1$ PSF are performed as follows. We successively scale the $E1$ PSF, which is a function of
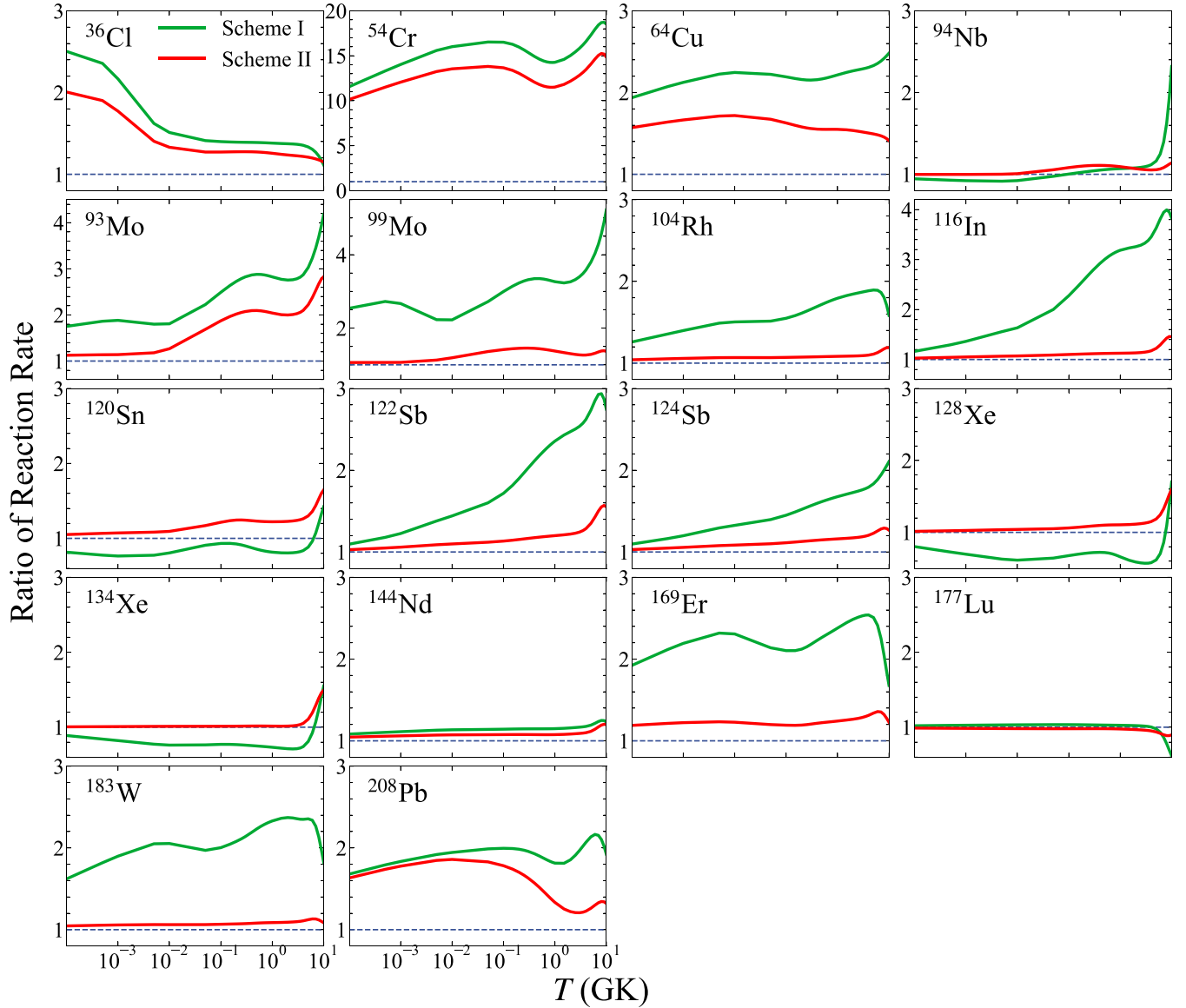
FIG. 2. Ratios of the neutron-capture reaction rates calculated with the $E1$ PSF of Scheme I (green lines) and Scheme II (red lines), respectively, to the one calculated with the microscopic $E1$ PSF.

the γ-ray energy E_γ, by a factor of 10 ($v_q = 10$) within an energy interval $\Delta E_\gamma = 0.5$ MeV from $E_\gamma = 0$ MeV to 10 MeV. As a result, we obtain the changed factors of the reaction rate and the corresponding sensitivities to the variations of the $E1$ PSF at different E_γ regions. At the temperature $T = 1$ GK, sensitivities of neutron-capture reaction rates to the variations of $E1$ PSF are shown in Fig. 5 for the Sn isotopes. It can be seen that all of the sensitive energy regions are unsurprisingly below the neutron separation energy. For most of the Sn isotopes, even with a variation at a small energy interval (0.5 MeV), the neutron-capture rates are quite sensitive to the variations of the $E1$ PSF. The reaction rate sensitivity of each nucleus in Fig. 5 represents an energy distribution which has a certain width and position. It indicates that there probably exists an effective energy window in which the $E1$ PSF is significant important to the calculations of the neutron-capture reaction rate. Obviously, these

windows are closely related to the productions of the emitted photons.

III. EFFECTIVE ENERGY WINDOW

A. Theoretical framework

To find out the effective energy window of the $E1$ PSF and formulate it, we start from the formula of the reaction rate with focus on the dominant dependence on the energy, especially on the energy of the emitting primary γ rays. In the astrophysical environment, the thermonuclear reaction rate of two nuclei is expressed by the Maxwellian-averaged rate $\langle \sigma v \rangle$ times the Avogadro number N_A,

$$N_A \langle \sigma v \rangle = \left(\frac{8}{\pi \mu} \right)^{1/2} \frac{N_A}{(k_B T)^{3/2}} \int_0^\infty E \sigma(E) e^{-E/k_B T} dE, \quad (3)$$
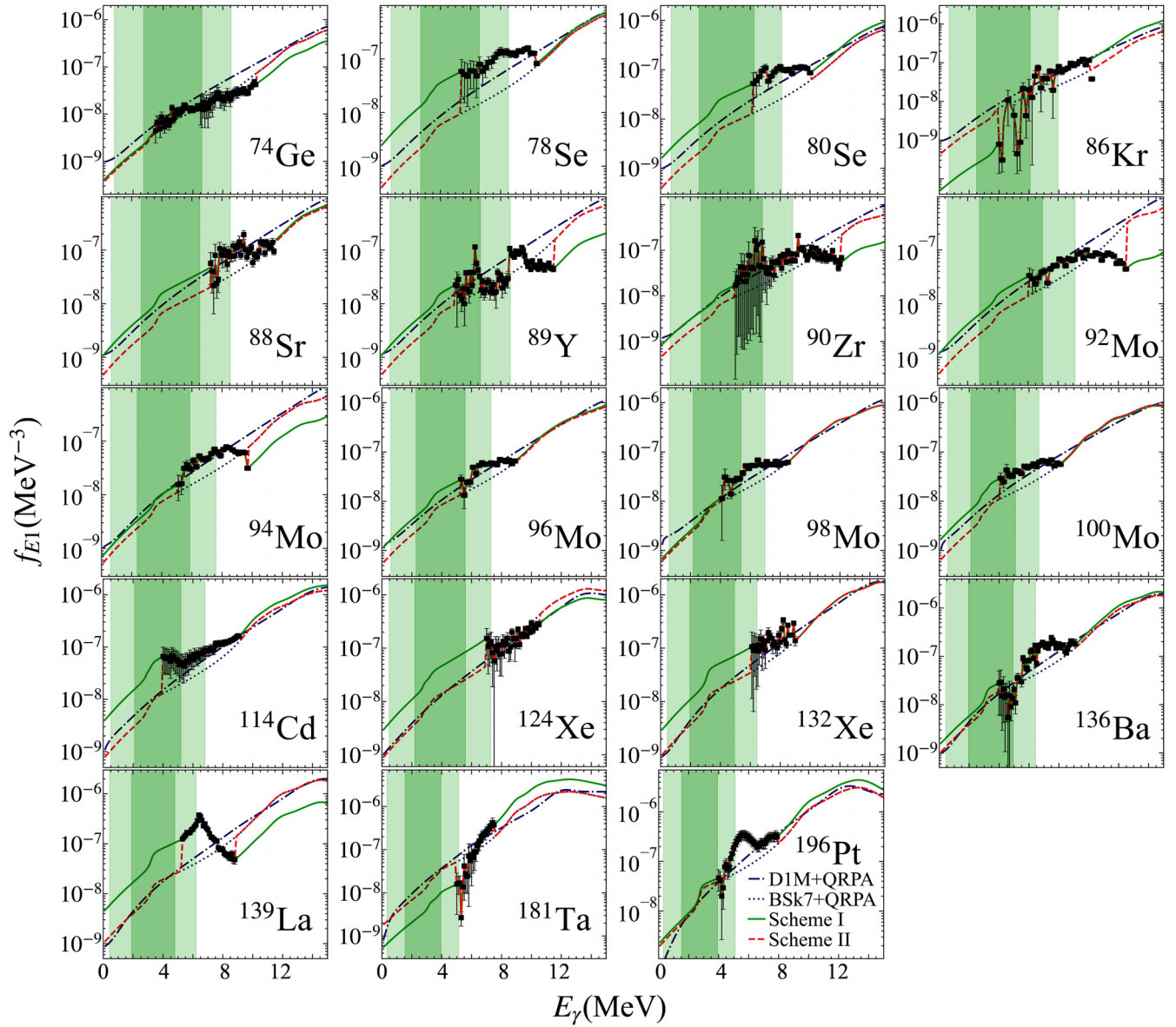
FIG. 3. Same as Fig. 1 for the experimental $E1$ PSF extracted from the total dipole PSF of the NRF data [40–54].

in which E is the incident energy, μ is the reduced mass, k_B is the Boltzmann constant, and T is the temperature. The neutron-capture cross section $\sigma(E)$ is usually estimated within the framework of the statistical Hauser-Feshbach model [5]. In this model, $\sigma(E)$ depends on the formation cross section of the compound nucleus $\sigma_C(E)$ and the primary γ-decay probability $P_\gamma(E, E_\gamma)$ which is a function of the γ-ray energy E_γ and the incident energy E. $P_\gamma(E, E_\gamma)$ is determined by the transmission coefficient $T(E_\gamma)$ of the photon and the level density $\rho(E, E_\gamma)$ of the residual nucleus after the primary γ transition,

$$P_\gamma(E, E_\gamma) \propto T(E_\gamma)\rho(E, E_\gamma). \tag{4}$$

With respect to the electric-dipole transition, the relationship between the transmission coefficient and the $E1$ PSF $f_{E1}(E_\gamma)$

can be expressed as

$$T(E_\gamma) \propto E_\gamma^3 f_{E1}(E_\gamma). \tag{5}$$

The phenomenological Fermi gas model [55] and its generalized forms [56–58] are most frequently used in describing the nuclear level density. The prominent feature of these models is the exponential dependence on the excitation energy. With this feature retained, the level density can be approximately expressed as

$$\rho(E, E_\gamma) \propto e^{2\sqrt{a(E+Q-E_\gamma)}}, \tag{6}$$

where a is the level density parameter of the residual nuclei and Q is the Q value of a reaction. Then the characteristic dependence of the γ-decay probability on the energy can be written as

$$P_\gamma(E, E_\gamma) \propto E_\gamma^3 f_{E1}(E_\gamma) e^{2\sqrt{a(E+Q-E_\gamma)}}. \tag{7}$$
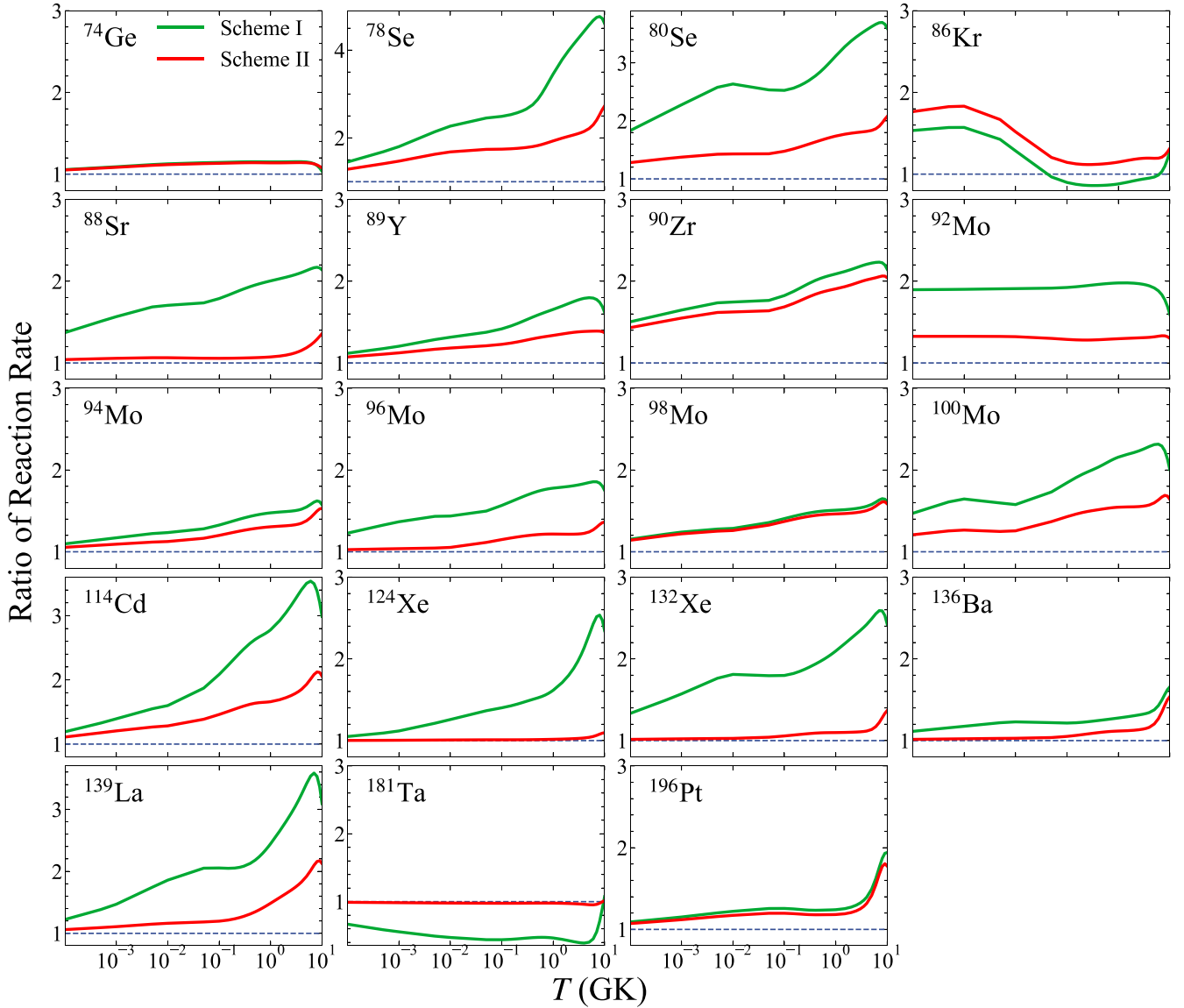
FIG. 4. Same as Fig. 2 for the $E1$ PSF taken from Fig. 3.

In the astrophysical situation, the effective incident energy window of a nuclear reaction with a neutron bombarding is mainly decided by the Maxwell-Boltzmann (MB) distribution with a peak at $E_{MB} = k_B T$ [59]. The important temperature at which production yields of r-process and i-process become sensitive to the neutron-capture cross section is less than 1.5 GK [4,60]. As a result, E_{MB} is far less than the Q value, and consequently the incident energy E in Eq. (7) can be omitted,

$$P_\gamma(E_\gamma) \propto E_\gamma^3 f_{E1}(E_\gamma) e^{2\sqrt{a(Q-E_\gamma)}}. \qquad (8)$$

The Brink-Axel hypothesis in the standard Lorentzian model [61,62] is widely used to calculate the dipole γ strength. Various generalized Lorentzian-type models of the $E1$ PSF have been developed to take into account the no-zero limit for the vanishing γ-ray energy and the energy-dependent width in the γ-ray strength [2,7,63–67]. Although these models behave differently in some aspects, their rising trends with

respect to the increasing γ-ray energy are basically similar below the neutron separation energy [9]. The improved description of the $E1$ PSF can be obtained using the microscopic model derived from the effective nucleon-nucleon interaction. Considerable differences between the microscopic PSF and the Lorentzian-type PSF can be found for the extreme neutron-rich nuclei, while for other isotopes, the microscopic predictions are close to the Lorentzian profile [10,11]. A recent study [67] indicates that the $E1$ PSF predicted by Lorentzian-type model is of versatility and flexibility for most nuclei. Therefore, we use the phenomenological standard Lorentzian form

$$f_{E1}(E_\gamma) \propto \frac{E_\gamma}{\left(E_\gamma^2 - E_r^2\right)^2 + E_\gamma^2 \Gamma_r^2}, \qquad (9)$$

where Γ_r and E_r are the width and the centroid energy of the giant dipole resonance, respectively. Because both the width
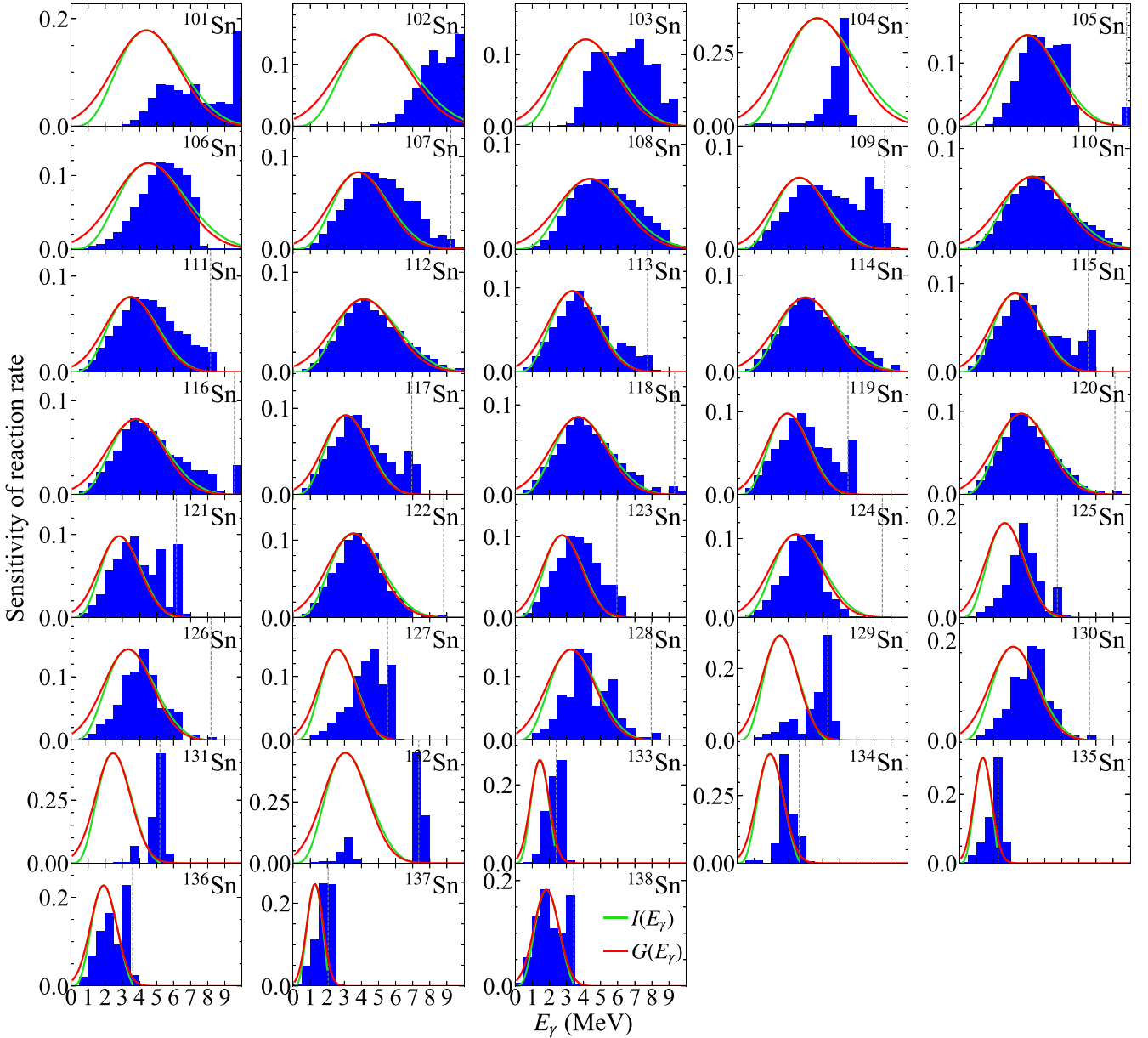
FIG. 5. (Blue bars) Sensitivities of the neutron-capture reaction rate to the variations of the $E1$ PSF at different E_γ energies from 1 MeV to 10 MeV for Sn isotopes, at the temperature $T = 1$ GK. Element annotations in each subgraph are the compound nuclei and grey dashed lines are the locations of their neutron separation energies. Green and red lines are the functions $I(E_\gamma)$ and $G(E_\gamma)$ of the effective energy window, respectively.

Γ_r and the γ-ray energy E_γ are generally much smaller than the centroid energy E_r under the environment encountered in astrophysics, the $E1$ PSF can be approximated as

$$f_{E1}(E_\gamma) \propto \frac{E_\gamma}{E_r^4 + E_\gamma^2 \Gamma_r^2} \approx \frac{E_\gamma}{E_r^4}. \qquad (10)$$

Substituting the $f_{E1}(E_\gamma)$ in Eq. (8) with Eq. (10), we finally obtain the predominant dependence on the emitted photon energy, and define this relationship as a function

$$I(E_\gamma) = I_m E_\gamma^4 e^{2\sqrt{a(Q-E_\gamma)}}, \qquad (11)$$

where I_m is a constant. This function, to a certain extent, represents the production of the photons at different emitted energies.

In general, variations of the $E1$ PSF at the energy region with larger photon production should have more impact on the reaction rates than variations in other energy regions. It implies that the function $I(E_\gamma)$ should be a description of the contributions of the $E1$ PSF at different photon energies to the reaction rates. Additionally, $I(E_\gamma)$ is a confined function with the maximum at the energy
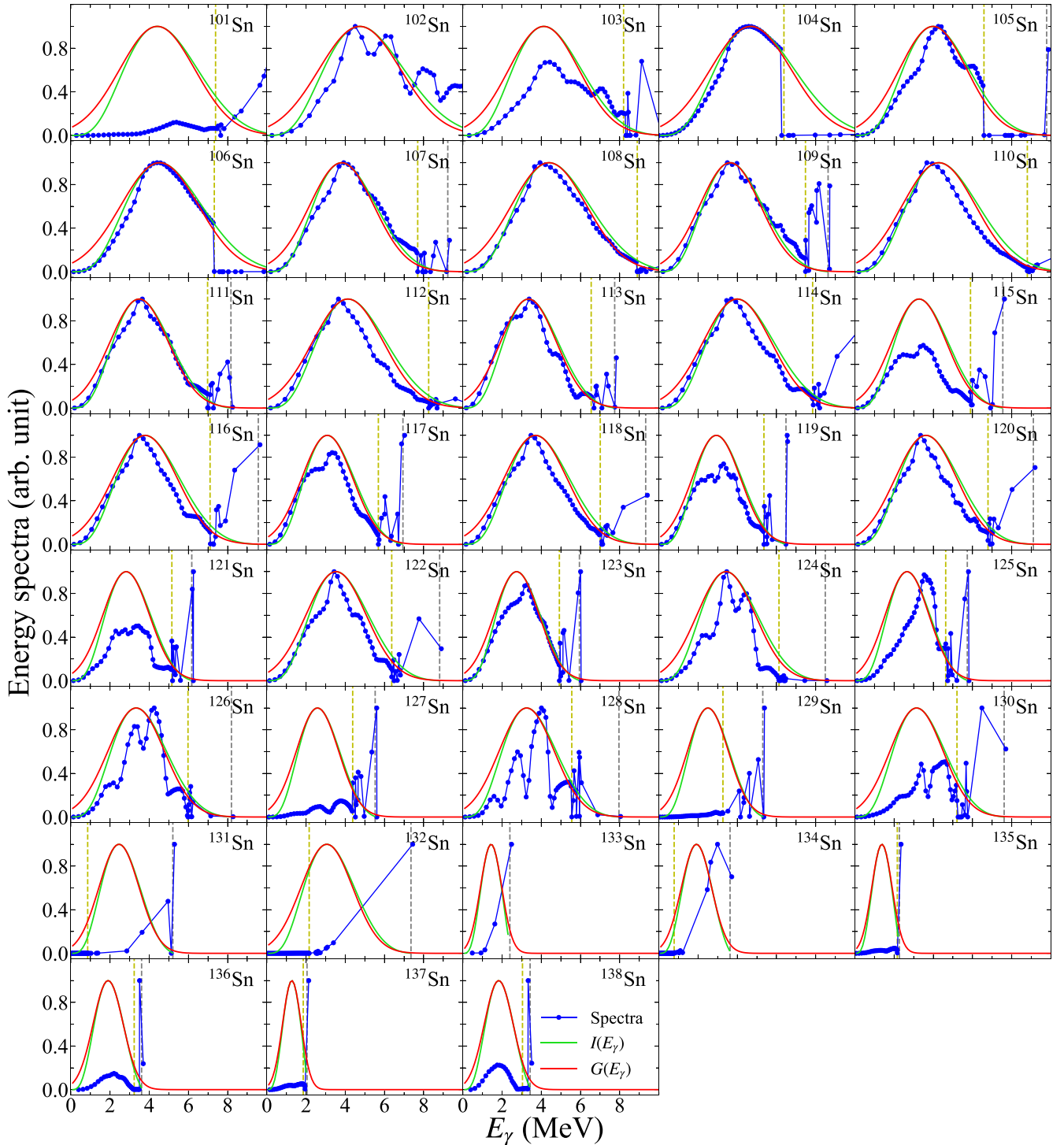
$$E_0 = \frac{4}{a}(\sqrt{4 + aQ} - 2). \qquad (12)$$

FIG. 6. Comparisons between the effective energy windows (green and red solid lines) and the primary γ-ray energy spectra (blue circles) for neutron-capture reactions on Sn isotopes, at an incident energy of 0.086 MeV. Element annotations in each subgraph are compound nuclei. Grey dashed lines are neutron separation energies. Yellow dashed lines are emitted photon energies for transition to the maximum discrete level.

Therefore the function $I(E_\gamma)$ represents an effective energy window in which the contributions of the $E1$ PSF to the reaction rate at E_0 reach to the maximum, and decrease gradually on either side of the peak. This function, however, is

not symmetrical around E_0. In order to easily distinguish different energy ranges according to their contributions and conveniently get the width of the effective energy window, a Gaussian function $G(E_\gamma)$ is used to approximate the function

$I(E_\gamma)$ with setting their peaks at the same E_0,

$$G(E_\gamma) = G_m \exp\left[\frac{-4(E_\gamma - E_0)^2}{\Delta^2}\right], \qquad (13)$$

where G_m and Δ are the maximal value and the full width at the $1/e$ of the maximum, respectively. Assuming that the curvatures of these two functions are same at $E_\gamma = E_0$, one can obtain

$$\Delta^2 = \frac{4E_0^2}{2 + E_0/(Q - E_0)}. \qquad (14)$$

The standard deviation σ of the Gaussian function can be expressed as $\sigma = \Delta/\sqrt{8}$.

As a result, we obtain an effective energy window characterized by a peak at E_0 and a width Δ wherein the contribution of the $E1$ PSF greatly impacts the astrophysical neutron-capture reaction rates. As the reaction energy Q can be obtained from experimental data or the mass formula, the values of E_0 and Δ depend only on the adjustable level density parameter a, in MeV^{-1}. In the theoretical framework of the Fermi gas model for level density, the parameter a is related to the density of single-particle states on the Fermi surface and can be approximated as $a = \alpha A$, where A is the mass number and α is a free parameter [9]. The parameters I_m and G_m in Eqs. (11) and (13), characterizing the height of the window, can be arbitrarily selected in the present discussions, because we are focused on the relative contributions from the $E1$ PSF to the reaction rate at different γ-ray energies. In the following analysis, these two parameters will be chosen to match the height of the window to the maximum values of the sensitivities or the primary γ-ray energy spectra.

B. Results and discussions

In order to test the reliability of the effective energy window, the following calculations, for comparisons, are performed by using the microscopic nuclear ingredients which differ from the phenomenological models and assumptions used to derive the window. These ingredients include the BSk7 + QRPA model for the $E1$ PSF, the HFB plus a combinatorial approach [68] for the level density, and the Bruyères Jeukenne-Lejeune-Mahaux optical model [69,70] for the nuclear potential.

The comparisons between the effective energy window defined by the functions $I(E_\gamma)$ and $G(E_\gamma)$ and the sensitivities of the reaction rate to the $E1$ PSF for Sn isotopes are shown in Fig. 5. Here, the parameter α is taken as $1/18\,MeV^{-1}$ for the optimal description of the sensitivities for most Sn isotopes, and this value will be used in the following calculations. One can see that the functions $I(E_\gamma)$ and $G(E_\gamma)$ exhibit good agreement with each other for all isotopes, thereby affirming the reliability of the Gaussian approximation to the effective energy window. Furthermore, as illustrated in Fig. 5, the sensitivities, although calculated based on the microscopic models of the PSF and the level density, can be effectively described by the effective energy window with consistent widths and positions for most Sn isotopes.

The primary γ-ray energy spectra are the experimental observables that represent the joint contributions from the PSF
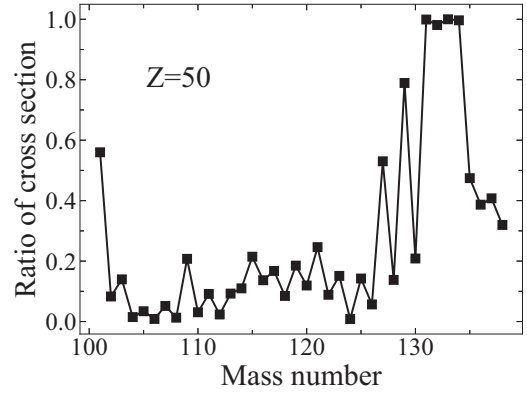

FIG. 7. Ratio of the cross section for transitions to discrete levels to the total cross section as a function of mass number for the Sn isotopic chain, at an incident energy of 0.086 MeV.

and the nuclear level density to the reaction cross sections (or reaction rates). Meanwhile, the effective energy window is obtained based on the product of the PSF and the level density. Hence, it is interesting to compare the primary γ-ray energy spectra calculated by microscopic nuclear ingredients with the effective energy window deduced from phenomenological models, and such comparison can further verify the reliability of this window. In Fig. 6, we calculate the primary γ-ray energy spectra of the neutron-capture reaction on Sn isotopes at an incident energy of 0.086 MeV, which corresponds to the peak of the Maxwell-Boltzmann distribution at the temperature $T = 1$ GK. In these calculations, the level density model is applied to the description of nuclear level spectrum, and ten discrete experimental levels are adopted for the low-lying levels if available.

It can be seen in Fig. 6 that for most isotopes, the effective energy windows well explain the shapes of the energy spectra of primary γ-ray transitions to the continuum levels (below the yellow dashed line). However, the energy spectra of transition to the discrete levels (between the yellow dashed line and the grey dashed line) are different from the windows. That is because the effective energy window is derived from the level density formula based on statistical assumptions and does not account for the discrete levels. Figure 7 shows the ratios of the cross section of the transitions to discrete levels to the total cross section in the neutron-capture reaction on Sn isotopes. One can see that, for most isotopes not near the neutron magic numbers, discrete levels contribute less than 25% to the total cross section. However, around $N = 50$ and 82, these contributions become highly significant and even dominant, primarily due to the challenges of exciting the nuclei near the magic numbers. These effects of the discrete levels are considered to be responsible for the discrepancies between the effective energy windows and the sensitivities in Fig. 5 (or the spectra in Fig. 6) for the nuclei near the magic numbers, such as $^{131-133}$Sn. In summary, because of the purely statistical assumptions and models employed in the theoretical derivation of the effective energy window, it is clear that this effective energy window can be applied to the neutron-capture reactions in which the contributions from continuum levels are dominant.
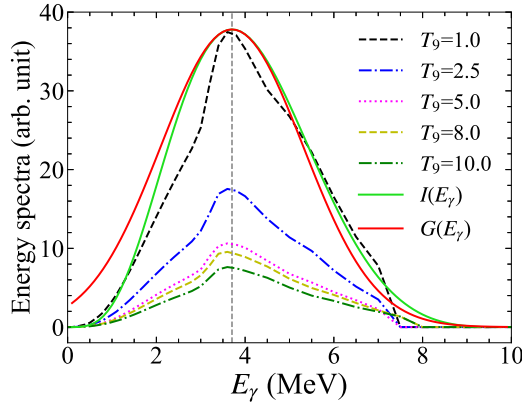
FIG. 8. Comparisons between the effective energy window of the $E1$ PSF and several primary γ-ray energy spectra for the reaction ^{117}Sn(n, γ) ^{118}Sn. Green and red solid lines are the functions $I(E_\gamma)$ and $G(E_\gamma)$ of the effective energy window, respectively. Five temperatures in the range of $T_9 = 1.0$ to 10.0 correspond to the primary γ-ray energy spectra with taking the incident energies at five Maxwell-Boltzmann peaks $k_B T_9$, respectively.

To investigate the applicability of the effective energy window in various astrophysical environments of the neutron capture, we calculate the primary γ-ray energy spectra for the reaction ^{117}Sn(n, γ) ^{118}Sn at five incident energies, which correspond to the peaks of five Maxwell-Boltzmann distributions within the temperature range of 1 GK to 10 GK. Comparisons between these spectra and the effective energy window are shown in Fig. 8. As can be seen, the widths of these spectra, as well as the locations of their peaks, are nearly identical at five typical incident energies in astrophysical environments, and they can be described by the effective energy window. These facts indicate that the effective energy window is an effective extraction of some common features from the energy spectra and can be applied to the general astrophysical environments of neutron captures due to the weak dependence on temperature.

Seventeen most critical and uncertain neutron-capture reactions for i-process nucleosynthesis between Ba and Pb are proposed in Ref. [3]. Most of these reaction rates are not known experimentally. The precision of these reactions is significantly impacted by the uncertainties of the PSFs. We predict the effective energy windows for these reactions in
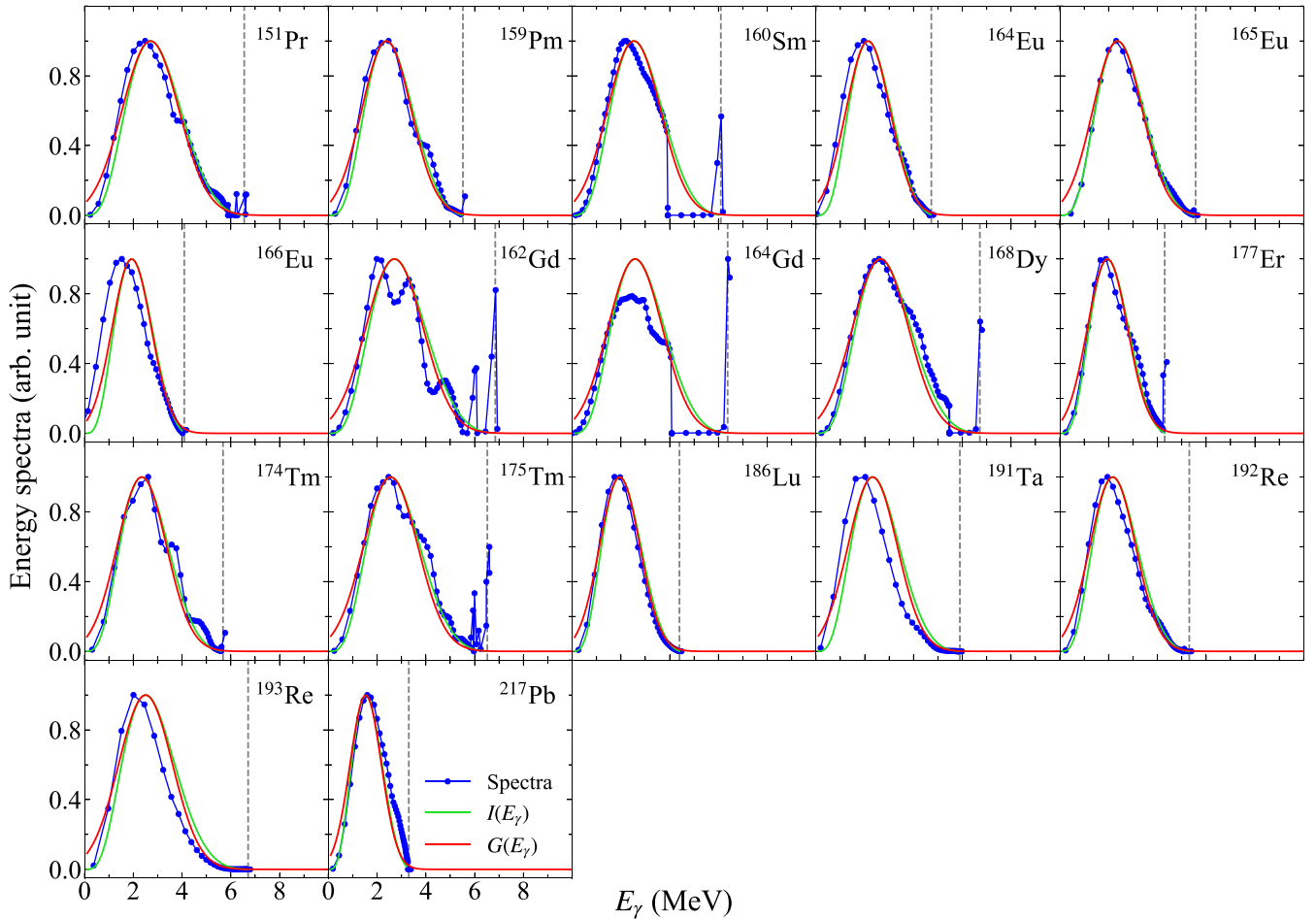

FIG. 9. Predictions of the effective energy window (green and red solid lines) for the most critical and uncertain neutron-capture reactions between Ba and Pb along the i-process path. Blue circles are the primary γ-ray energy spectra at an incident energy corresponding to the Maxwell-Boltzmann peak at a temperature of $T = 250$ MK.

Fig. 9. As can be seen, the windows agree well with the calculated primary γ-ray energy spectra for all these nuclei. This means that for the critical nuclei in *i*-process, the important energy range of the $E1$ PSF can be reasonably predicted using the effective energy window.

Using the Gaussian function $G(E_\gamma)$ of the effective energy window, we can conveniently get several specific energy ranges of the $E1$ PSF centered around the Gaussian peak. Both one σ and two σ energy ranges are depicted in Figs. 1 and 3, compared with the measured $E1$ PSF data. It can be seen that the experimental data only partially fall into these important ranges. More efforts are needed in the future to expand the experimental measurements of the $E1$ PSFs into these energy ranges.

IV. CONCLUSIONS

The impacts of uncertainties in the $E1$ PSFs on astrophysical neutron-capture reaction rates are investigated systematically through combining available experimental data with theoretical predictions by two schemes. It is found that large uncertainties in the $E1$ PSF significantly affect the precision of neutron-capture reaction rate estimates. In order to find out the most important energy range of the $E1$ PSF, we analyze the sensitivities of the neutron-capture reaction rate to variations in the $E1$ PSF at different γ-ray energies for the Sn isotopes. The results indicate that there probably exist an effective energy window with a certain width and position within which variations in the $E1$ PSF have a significant impact on the astrophysical neutron-capture reaction rate.

We derive a function $I(E_\gamma)$ from the reaction rate formula to describe the effective energy window and approximate it with a Gaussian function $G(E_\gamma)$, for the convenience of drawing the width of this window. The consistency between the effective energy windows and the sensitivities of astrophysical rates is found for most Sn isotopes. Further analysis on the primary γ-ray energy spectra for Sn isotopes indicates that the effective energy window can be applied to the nuclei which have dominant transitions to the continuum levels in the neutron-capture reactions. Several primary γ-ray energy spectra for the reaction $^{117}\mathrm{Sn}(n,\gamma)^{118}\mathrm{Sn}$ are calculated specifically at five typical incident energies corresponding to five astrophysical temperatures. It is found that the energy spectra are weakly dependent on the incident energies and thus the effective energy window can be used to the general astrophysical environments of neutron captures. Furthermore, we test the effective energy windows for critical reactions in the *i*-process and find that reasonable predictions for the effective energy range of the $E1$ PSF can be provided by the windows. By using the Gaussian function of the effective energy window, several specific effective energy ranges can be conveniently obtained according to their contributions to the reaction rates. However, currently available experimental data of the $E1$ PSF do not completely cover these important effective energy ranges. Further research efforts are needed in both theory and experiments to give precise descriptions of the $E1$ PSF in these proposed ranges.

[1] M. Arnould, S. Goriely, and K. Takahashi, Phys. Rep. **450**, 97 (2007).

[2] S. Goriely, Phys. Lett. B **436**, 10 (1998).

[3] A. Choplin, L. Siess, and S. Goriely, EPJ Web Conf. **279**, 07001 (2023).

[4] S. Goriely, L. Siess, and A. Choplin, Astron. Astrophys. **654**, A129 (2021).

[5] W. Hauser and H. Feshbach, Phys. Rev. **87**, 366 (1952).

[6] G. A. Bartholomew, E. D. Earle, A. J. Fergusson, J. W. Knowles, and M. A. Lone, Adv. Nuclear Phys. **7**, 229 (1973).

[7] J. Kopecky and M. Uhl, Phys. Rev. C **41**, 1941 (1990).

[8] S. Goriely, P. Dimitriou, M. Wiedeking, T. Belgya, R. Firestone, J. Kopecky, M. Krtička, V. Plujko, R. Schwengner, S. Siem *et al.*, Eur. Phys. J. A **55**, 172 (2019).

[9] R. Capote, M. Herman, P. Obložinský, P. G. Young, S. Goriely, T. Belgya, A. V. Ignatyuk, A. J. Koning, S. Hilaire, V. A. Plujko *et al.*, Nucl. Data Sheets **110**, 3107 (2009).

[10] S. Goriely and E. Khan, Nucl. Phys. A **706**, 217 (2002).

[11] S. Goriely, E. Khan, and M. Samyn, Nucl. Phys. A **739**, 331 (2004).

[12] I. Daoutidis and S. Goriely, Phys. Rev. C **86**, 034328 (2012).

[13] M. Martini, S. Péru, S. Hilaire, S. Goriely, and F. Lechaftois, Phys. Rev. C **94**, 014304 (2016).

[14] Y. Xu, S. Goriely, and E. Khan, Phys. Rev. C **104**, 044301 (2021).

[15] S. Goriely, S. Hilaire, S. Péru, and K. Sieja, Phys. Rev. C **98**, 014327 (2018).

[16] K. L. Malatji, K. S. Beckmann, M. Wiedeking, S. Siem, S. Goriely, A. C. Larsen, K. O. Ay, F. L. Bello Garrote, L. C. Campo, A. Görgen, V. W. Ingeberg, P. Jones, B. V. Kheswa, P. von Neumann-Cosel, M. Ozgur, G. Potel, L. Pellegri, T. Renstrom, G. M. Tveten, and F. Zeiser, Phys. Rev. C **103**, 014309 (2021).

[17] F. Pogliano, F. L. Bello Garrote, A. C. Larsen, H. C. Berg, D. Gjestvang, A. Görgen, M. Guttormsen, V. W. Ingeberg, T. W. Johansen, K. L. Malatji, E. F. Matthews, M. Markova, J. E.

Midtbo, V. Modamio, L. G. Pedersen, E. Sahin, S. Siem, T. G. Tornyi, and A. S. Voyles, Phys. Rev. C **107**, 034605 (2023).

[18] F. Pogliano, A. C. Larsen, S. Goriely, L. Siess, M. Markova, A. Görgen, J. Heines, V. W. Ingeberg, R. G. Kjus, J. E. L. Larsson, K. C. W. Li, E. M. Martinsen, G. J. Owens-Fryar, L. G. Pedersen, S. Siem, G. S. Torvund, and A. Tsantiri, Phys. Rev. C **107**, 064614 (2023).

[19] T. Rauscher, Astrophys. J. Suppl. Series **201**, 26 (2012).

[20] A. J. Koning, S. Hilaire, and M. C. Duijvestijn, in *Proceedings of the International Conference on Nuclear Data for Science and Technology*, edited by O. Bersillon *et al.* (EDP Sciences, Les Ulis, France, 2008).

[21] S. Goriely, S. Hilaire, and A. J. Koning, Astron. Astrophys. **487**, 767 (2008).

[22] Y. Xu, S. Goriely, A. J. Koning, and S. Hilaire, Phys. Rev. C **90**, 024604 (2014).

[23] IAEA, Photon Strength Function Database (2022), https://www-nds.iaea.org/PSFdatabase.

[24] T. Rauscher, Int. J. Mod. Phys. E **20**, 1071 (2011).

[25] R. E. Chrien and J. Kopecký, Phys. Rev. Lett. **39**, 911 (1977).

[26] C. Coceva, Il Nuovo Cimento A **107**, 85 (1994).

[27] W. Stein, B. W. Thomas, and E. R. Rae, Phys. Rev. C **1**, 1468 (1970).

[28] R. E. Chrien, K. Rimawi, and J. B. Garg, Phys. Rev. C **3**, 2054 (1971).

[29] O. A. Wasson and G. G. Slaughter, Phys. Rev. C **8**, 297 (1973).

[30] R. E. Chrien, G. W. Cole, G. G. Slaughter, and J. A. Harvey, Phys. Rev. C **13**, 578 (1976).

[31] K. Rimavi, J. B. Garg, R. E. Chrien, and R. G. Graves, Phys. Rev. C **2**, 1793 (1970).

[32] F. Corvi and M. Stefanon, Nucl. Phys. A **233**, 185 (1974).

[33] A. Tamii, I. Poltoratska, P. von Neumann-Cosel, Y. Fujita, T. Adachi, C. A. Bertulani, J. Carter, M. Dozono, H. Fujita, K. Fujita *et al.*, Phys. Rev. Lett. **107**, 062502 (2011).

[34] I. Poltoratska, P. von Neumann-Cosel, A. Tamii, T. Adachi, C. A. Bertulani, J. Carter, M. Dozono, H. Fujita, K. Fujita, Y. Fujita *et al.*, Phys. Rev. C **85**, 041304(R) (2012).

[35] A. Lottin and D. Paya, J. Phys. (Paris) **32**, 849 (1971).

[36] R. Massarczyk, G. Rusev, R. Schwengner, F. Dönau, C. Bhatia, M. E. Gooden, J. H. Kelley, A. P. Tonchev, and W. Tornow, Phys. Rev. C **90**, 054310 (2014).

[37] C. M. McCullagh, PhD thesis, Stony Brook University, 1979.

[38] J. B. Garg, G. W. Cole, H. I. Liou, and R. E. Chrien, Phys. Rev. C **13**, 1139 (1976).

[39] F. Becvar, J. Honzatko, M. E. Montero-Cabrera, S. A. Telezhnikov, and H. T. Hiep, Yad. Fiz. **46**, 392 (1987).

[40] R. Massarczyk, R. Schwengner, L. A. Bernstein, M. Anders, D. Bemmerer, R. Beyer, Z. Elekes, R. Hannaske, A. R. Junghans, T. Kögler, M. Roder, K. Schmidt, A. Wagner, and L. Wagner, Phys. Rev. C **92**, 044309 (2015).

[41] G. Schramm, R. Massarczyk, A. R. Junghans, T. Belgya, R. Beyer, E. Birgersson, E. Grosse, M. Kempe, Z. Kis, K. Kosev *et al.*, Phys. Rev. C **85**, 014311 (2012).

[42] A. Makinaga, R. Massarczyk, M. Beard, R. Schwengner, H. Otsu, T. Al-Abdullah, M. Anders, D. Bemmerer, R. Hannaske, R. John *et al.*, Phys. Rev. C **94**, 044304 (2016).

[43] R. Schwengner, R. Massarczyk, G. Rusev, N. Tsoneva, D. Bemmerer, R. Beyer, R. Hannaske, A. R. Junghans, J. H. Kelley, E. Kwan *et al.*, Phys. Rev. C **87**, 024306 (2013).

[44] R. Schwengner, G. Rusev, N. Benouaret, R. Beyer, M. Erhard, E. Grosse, A. R. Junghans, J. Klug, K. Kosev, L. Kostov *et al.*, Phys. Rev. C **76**, 034321 (2007).

[45] N. Benouaret, R. Schwengner, G. Rusev, F. Dönau, R. Beyer, M. Erhard, E. Grosse, A. R. Junghans, K. Kosev, C. Nair, K. D. Schilling, A. Wagner, and N. Bendjaballah, Phys. Rev. C **79**, 014303 (2009).

[46] R. Schwengner, G. Rusev, N. Tsoneva, N. Benouaret, R. Beyer, M. Erhard, E. Grosse, A. R. Junghans, J. Klug, K. Kosev *et al.*, Phys. Rev. C **78**, 064314 (2008).

[47] G. Rusev, R. Schwengner, R. Beyer, M. Erhard, E. Grosse, A. R. Junghans, K. Kosev, C. Nair, K. D. Schilling, A. Wagner *et al.*, Phys. Rev. C **79**, 061302(R) (2009).

[48] G. Rusev, R. Schwengner, F. Dönau, M. Erhard, E. Grosse, A. R. Junghans, K. Kosev, K. D. Schilling, A. Wagner, F. Bečvář, and M. Krticka, Phys. Rev. C **77**, 064321 (2008).

[49] R. Massarczyk, G. Schramm, T. Belgya, R. Schwengner, R. Beyer, D. Bemmerer, Z. Elekes, E. Grosse, R. Hannaske, A. R. Junghans *et al.*, Phys. Rev. C **93**, 014301 (2016).

[50] R. Massarczyk, R. Schwengner, F. Dönau, S. Frauendorf, M. Anders, D. Bemmerer, R. Beyer, C. Bhatia, E. Birgersson, M. Butterling, Z. Elekes, A. Ferrari, M. E. Gooden, R. Hannaske, A. R. Junghans, M. Kempe, J. H. Kelley, T. Kogler, A. Matic, M. L. Menzel, S. Muller, T. P. Reinhardt, M. Roder, G. Rusev, K. D. Schilling, K. Schmidt, G. Schramm, A. P. Tonchev, W. Tornow, and A. Wagner, Phys. Rev. Lett. **112**, 072501 (2014).

[51] R. Massarczyk, R. Schwengner, F. Dönau, E. Litvinova, G. Rusev, R. Beyer, R. Hannaske, A. R. Junghans, M. Kempe, J. H. Kelley, T. Kogler, K. Kosev, E. Kwan, M. Marta, A. Matic, C. Nair, R. Raut, K. D. Schilling, G. Schramm, D. Stach, A. P. Tonchev, W. Tornow, E. Trompler, A. Wagner, and D. Yakorev, Phys. Rev. C **86**, 014319 (2012).

[52] A. Makinaga, R. Schwengner, G. Rusev, F. Dönau, S. Frauendorf, D. Bemmerer, R. Beyer, P. Crespo, M. Erhard, A. R. Junghans, J. Klug, K. Kosev, C. Nair, K. D. Schilling, and A. Wagner, Phys. Rev. C **82**, 024314 (2010).

[53] A. Makinaga, R. Massarczyk, R. Schwengner, M. Beard, F. Dönau, M. Anders, D. Bemmerer, R. Beyer, R. Hannaske, A. R. Junghans *et al.*, Phys. Rev. C **90**, 044301 (2014).

[54] R. Massarczyk, G. Schramm, A. R. Junghans, R. Schwengner, M. Anders, T. Belgya, R. Beyer, E. Birgersson, A. Ferrari, E. Grosse *et al.*, Phys. Rev. C **87**, 044306 (2013).

[55] H. A. Bethe, Rev. Mod. Phys. **9**, 69 (1937).

[56] W. Dilg, W. Schantl, H. Vonach, and M. Uhl, Nucl. Phys. A **217**, 269 (1973).

[57] A. Gilbert and A. G. W. Cameron, Can. J. Phys. **43**, 1446 (1965).

[58] A. J. Koning, S. Hilaire, and S. Goriely, Nucl. Phys. A **810**, 13 (2008).

[59] T. Rauscher, Phys. Rev. C **81**, 045807 (2010).

[60] M. Mumpower, R. Surman, G. C. McLaughlin, and A. Aprahamian, Prog. Part. Nucl. Phys. **86**, 86 (2016).

[61] D. Brink, Ph.D. thesis, University of Oxford, 1955.

[62] P. Axel, Phys. Rev. **126**, 671 (1962).

[63] S. G. Kadmenskii, V. P. Markushev, and V. I. Furmann, Yad. Fiz. **37**, 277 (1983).

[64] J. Kopecky, M. Uhl, and R. E. Chrien, Phys. Rev. C **47**, 312 (1993).

[65] S. F. Mughabghab and C. L. Dunford, Phys. Lett. B **487**, 155 (2000).

[66] V. A. Plujko, O. M. Gorbachenko, R. Capote, and P. Dimitriou, At. Data Nucl. Data Tables **123–124**, 1 (2018).

[67] S. Goriely and V. Plujko, Phys. Rev. C **99**, 014303 (2019).

[68] S. Goriely, S. Hilaire, and A. J. Koning, Phys. Rev. C **78**, 064307 (2008).

[69] E. Bauge, J. P. Delaroche, and M. Girod, Phys. Rev. C **63**, 024607 (2001).

[70] J. P. Jeukenne, A. Lejeune, and C. Mahaux, Phys. Rev. C **16**, 80 (1977).